ELSEVIER

Journal of Nuclear Materials 303 (2002) 34–43

journal of nuclear materials

www.elsevier.com/locate/jnucmat

Temperature effects on the mechanical properties of candidate SNS target container materials after proton and neutron irradiation

T.S. Byun [a,*], K. Farrell [a], E.H. Lee [a,1], L.K. Mansur [a], S.A. Maloy [b], M.R. James [b], W.R. Johnson [c]

[a] *Metal and Ceramics Division, Oak Ridge National Laboratory, Building 4500S, P.O. Box 2008, MS-6151, Oak Ridge, TN 37831, USA*
[b] *Los Alamos National Laboratory, MS-H809, Los Alamos, NM 87545, USA*
[c] *General Atomics, P.O. Box 85608, San Diego, CA 92186, USA*

Received 21 November 2001; accepted 14 February 2002

Abstract

This report presents the tensile properties of EC316LN austenitic stainless steel and 9Cr–2WVTa ferritic/martensitic steel after 800 MeV proton and spallation neutron irradiation to doses in the range 0.54–2.53 dpa at 30–100 °C. Tensile testing was performed at room temperature (20 °C) and 164 °C. The EC316LN stainless steel maintained notable strain-hardening capability after irradiation, while the 9Cr–2WVTa ferritic/martensitic steel posted negative hardening in the engineering stress–strain curves. In the EC316LN stainless steel, increasing the test temperature from 20 to 164 °C decreased the strength by 13–18% and the ductility by 8–36%. The effect of test temperature for the 9Cr–2WVTa ferritic/martensitic steel was less significant than for the EC316LN stainless steel. In addition, strain-hardening behaviors were analyzed for EC316LN and 316L stainless steels. The strain-hardening rate of the 316 stainless steels was largely dependent on test temperature. A calculation using reduction of area measurements and stress–strain data predicted positive strain hardening during plastic instability..

1. Introduction

The container vessel for the mercury target of the proposed SNS is expected to operate at a temperature between 100 and 200 °C [1]. A goal exposure for the first target is six months operation, corresponding to a displacement dose of about 5 dpa in the container vessel. In earlier reports [2–7] we described the tensile properties of candidate vessel materials after irradiation in the Los Alamos Neutron Scattering Center (LANSCE) accelerator at Los Alamos National Laboratory (LANL) at temperatures in the range 58–160 °C. The tensile tests were conducted at ORNL at room temperature. Austenitic stainless steels showed the most satisfactory results. They retained significant ductility even after irradiation to 11 dpa; the EC316LN steel had positive work hardening and a uniform elongation of 6% [2,5]. Ferritic/martensitic steels displayed prompt instability failures at yield.

In the same LANSCE experiment, other materials were irradiated and tested by LANL for consideration for use in their Accelerator Production of Tritium (APT) project [8–10]. Two stainless steels, 316L and 304L, were tested at 50, 80 and 164 °C, and they showed greater ductility losses than for ORNL's austenitic steels [6,7]. In LANL's engineering stress–strain data, all stainless steel specimens that were irradiated to doses higher

* Corresponding author. Tel.: +1-865 576 7738; fax: +1-865 574 0641.
E-mail address: byunts@ornl.gov (T.S. Byun).
[1] Present address: Honeywall Electronics Materials, 1349 Moffett Park Dr., Sunnyvale, CA 94089, USA.

0022-3115/02/$ - see front matter.
PII: S0022-3115(02)00806-1

than 2 dpa and tested at 80 or 164 °C showed nearly zero or negative strain hardening, and almost no uniform elongation. Comparison with the ORNL data suggested that test temperature was obviously an important factor in reduced ductility [6,7,11–13], but the role of chemical composition of the steels was unclear. Subsequent tests at LANL [6] established that test temperature overrules effects of chemical composition in the LANL austenitic steels.

To confirm the temperature effects on tensile properties for the SNS candidate materials, tensile tests on a few available specimens of the irradiated EC316LN austenitic steel and a 9Cr–2WVTa ferritic/martensitic steel were performed at room temperature and 164 °C. The latter temperature was chosen to conform to LANL's highest test temperature. This report presents the tensile test results, focusing on the effects of test temperature on tensile properties. In addition, detailed analyses on strain-hardening behaviors are performed for the uniform and localized deformation regimes of ORNL's EC316LN and LANL's 316L stainless steels. No detailed analysis was performed for the strain-hardening behaviors of the ferritic/martensitic steel because it showed prompt plastic instability after irradiation.

2. Experiments and analyses

Test materials were EC316LN austenitic stainless steel, where the letters EC indicate European Community, and 9Cr–2WVTa ferritic/martensitic steel. Table 1 lists their identities, chemical compositions, and heat treatments. SS-3 type tensile samples were irradiated and tested. The SS-3 tensile specimen is shown in Fig. 1. Its nominal gauge section dimensions are 7.6 mm long, 1.5 mm wide, and 0.76 mm thick.

For the present tensile testing, eight SS-3 tensile specimens were irradiated at two different positions in Tube 4 of Insert 17A, an in-beam position of the LANSCE–APT irradiation setup [8–10]. In the irradiation experiment, specimens were irradiated with a beam of 800 MeV protons at an average current of 1 mA and

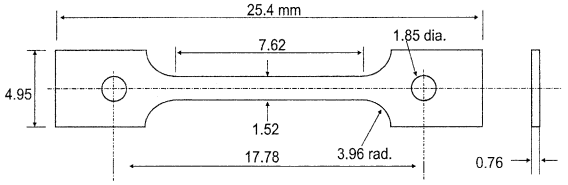

Fig. 1. Dimensions of SS-3 tensile specimen.

with spallation neutrons [14,15] emitted from a tungsten target. After irradiation, the irradiation conditions for each specimen were calculated using the LAHET code system [16,17] from analysis of pure metal activation foils [18]. The exposure for each specimen was dependent on its radial and axial position relative to the beam center and the tungsten target. The doses evaluated were 0.54 and 1.87 dpa for EC316LN steel specimens and 0.52 and 2.53 dpa for 9Cr–2WVTa steel specimens. He and H productions were in the range of 40–200 appm and 200–1600 appm, respectively. Irradiation temperatures were in the range 30–100 °C. These irradiation conditions are summarized in Table 2, and additional information on the LANSCE–APT experiment is given in previous reports [8,10].

Tensile testing was performed at room temperature (20 °C) and an elevated temperature (164 °C) in a screw-driven machine at a crosshead speed of 0.008 mm/s, corresponding to a nominal strain rate of 10^{-3} s^{-1}. An unirradiated gauge length of 7.6 mm was taken as the reference gauge length for calculation of engineering and true strains. Engineering stresses were calculated as the load divided by initial cross-sectional area measured before irradiation. True stress (σ)–true strain (ε) data and strain-hardening rate ($d\sigma/d\varepsilon$) were calculated from the engineering stress–strain data and used to determine true uniform strains, or true strains to plastic instability. Strain-hardening analysis was also performed on the earlier tensile test data of LANL's 316L stainless steel [6,7] to compare with the new results for EC316LN stainless steel. Strain-hardening rates for necking deformation were predicted from measurements of reduction

Table 1
Compositions of test materials

Material	ID mark	Composition (wt%)										
		Bal.	Ni	Cr	Mo	Mn	Si	C	N	Nb	V	Other
EC316LN[a]	E	Fe	12.2	17.45	2.5	1.81	0.39	0.024	0.067			
9Cr–2WVTa steel (Ht. 3791)[b]	Q	Fe	<0.01	8.90	0.01	0.44	0.21	0.11	0.021	<0.01	0.23	2.01W; 0.06Ta

[a] Annealed 1 h @ 950 °C in vacuum.
[b] Wrapped in Zr foil and annealed 30 min @ 1050 °C in helium, fast cool; reheated 1 h @ 750 °C, fast cool.

Table 2
Irradiation conditions for SS-3 tensile specimens

ID mark	Material	Insert-Tube-Sandwich	Distance[a] (mm)	Height[a] (mm)	Irradiation temperature (°C)	dpa[b]	He (appm)	H (appm)	Proton fluence (10^{24} p/m^2)	Neutron fluence (10^{24} n/m^2)			
										$E < 0.1$ MeV	$0.1 < E <$ 20 MeV	$20 < E <$ 150 MeV	$E > 150$ MeV
E50	EC316LN	17A-4-6	15.2	3.0	94	1.87	133.1	1110.8	5.68	0.16	1.49	0.45	0.25
E51	EC316LN	17A-4-6	40.6	3.0	39	0.54	34.2	274.3	1.17	0.16	0.80	0.14	0.08
E54	EC316LN	17A-4-6	40.6	3.0	39	0.54	34.2	274.3	1.17	0.16	0.80	0.14	0.08
E55	EC316LN	17A-4-6	15.2	3.0	94	1.87	133.1	1110.8	5.68	0.16	1.49	0.45	0.25
Q19	9Cr–2WVTa	17A-4-6	−10.2	3.0	100	2.53	181.8	1522.2	8.04	0.21	1.57	0.68	0.24
Q20	9Cr–2WVTa	17A-4-6	−35.6	3.0	46	0.64	41.5	350.9	1.28	0.16	1.02	0.18	0.08
Q21	9Cr–2WVTa	17A-4-6	−10.2	3.0	100	2.53	181.8	1522.2	8.04	0.21	1.57	0.68	0.24
Q22	9Cr–2WVTa	17A-4-6	−35.6	3.0	46	0.64	41.5	350.9	1.28	0.16	1.02	0.18	0.08

[a] Positions of specimen centers from beam center; in the perpendicular directions to the beam direction.
[b] 5–25% were contributed from the neutrons.

of area (RA) and tensile test data for the 316L stainless steel [19]. The RA data were measured on the fracture surface using a scanning electron microscope.

3. Results and discussion

3.1. EC316LN austenitic stainless steel

Fig. 2 presents engineering stress–strain curves for EC316LN stainless steel. The engineering tensile data read from the curves are summarized in Table 3. The EC316LN stainless steel showed considerable radiation hardening and loss of ductility after irradiation. At both 20 and 164 °C the yield strengths at 1.87 dpa were three times higher than those for the unirradiated condition, and the uniform strain was reduced to about one fourth of its unirradiated value. Despite the loss in ductility the EC316LN stainless steel retained positive strain hardening after irradiation up to 1.87 dpa at both temperatures.

As expected, the EC316LN stainless steel showed significant temperature effects on tensile properties [6,7]. With increasing test temperature from 20 to 164 °C, the yield and ultimate tensile strengths (YS and UTS) decreased by 13–18% from their room temperature values. These percentage reductions in strengths seemed to be insensitive to irradiation dose between 0.5 and 1.9 dpa. The increase of test temperature also reduced the ductility of EC316LN stainless steel. The reduction in ductility was most pronounced in the unirradiated condition;

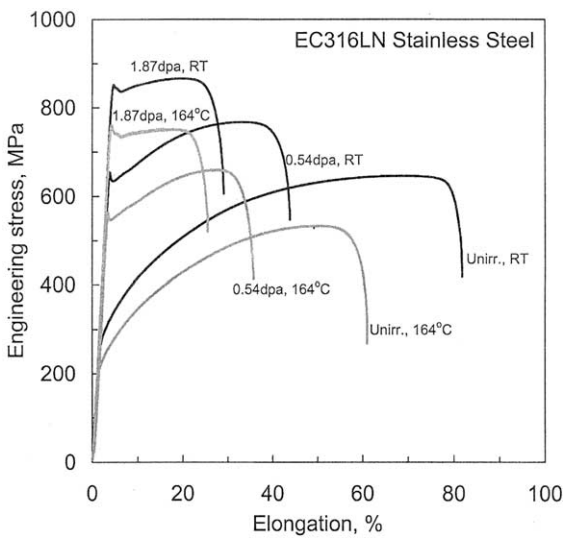

Fig. 2. Engineering stress–strain curves of EC316LN stainless steel after irradiation to labeled doses in spallation environments.

Table 3
Tensile properties of irradiated and unirradiated steels

Materials	ID mark	dpa	Irradiation temperature (°C)	Test temperature (°C)	YS (MPa)	UTS (MPa)	UE (%)	TE (%)
EC316LN	E19	0	–	20	279	645	68.6	78.0
	E51	0.54	39	20	636	769	30.0	39.5
	E50	1.87	94	20	837	865	15.7	23.7
	E12	0	–	164	239	532	50.6	59.0
	E54	0.54	39	164	550	658	24.9	31.6
	E55	1.87	94	164	740	750	14.5	20.9
9Cr–2VWTa	Q16	0	–	20	536	700	8.6	16.3
	Q20	0.64	46	20	881	[a]	0.1	7.2
	Q19	2.53	100	20	978	[a]	0.2	4.6
	Q17	0	–	164	526	641	6.9	14.7
	Q22	0.64	46	164	803	[a]	0.3	7.0
	Q21	2.53	100	164	880	[a]	0.1	4.0

UE: Uniform elongation; TE: Total elongation.
[a] UTS = YS.

Table 3 shows 26% reduction in uniform elongation and 24% reduction in total elongation. After irradiation to 1.87 dpa the percentage reductions in ductility due solely to the increase of temperature were about 8% and 12% for uniform and total elongations, respectively.

In Figs. 3 and 4 the tensile data for current EC316LN specimens are overlaid on the trend bands of the database for 316 stainless steels irradiated at temperatures between room temperature and 200 °C in fission reactors and tested in the same temperature range [20]. Further, the data are compared with the previous room temperature data for candidate SNS target container materials irradiated in neutron (n) or proton (p) areas of the LANSCE–APT irradiation [2–5]. At doses below about 1 dpa both yield strength and uniform elongation data for LANSCE irradiations are compatible with the trend bands of the database. At higher doses, however, the yield strengths of the LANSCE specimens tend to

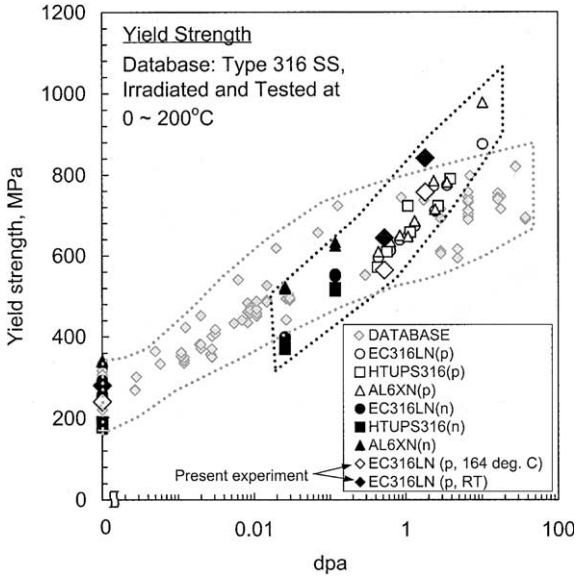

Fig. 3. Yield stresses of EC316LN stainless steel compared with database for 316 stainless steels irradiated in fission reactors and with room temperature data for austenitic stainless steels irradiated in spallation conditions (p and n denote proton and neutron dominant areas, respectively).

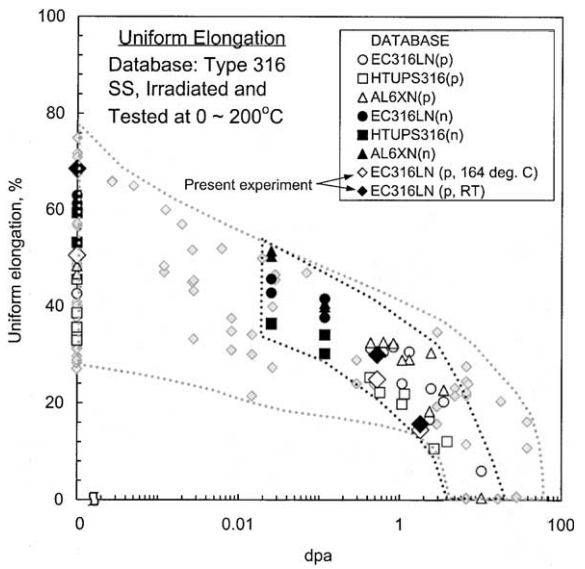

Fig. 4. Uniform elongations of EC316LN stainless steel compared with database for 316 stainless steels irradiated in fission reactors and with room temperature data for austenitic stainless steels irradiated in spallation conditions (p and n denote proton and neutron dominant areas, respectively).

exceed the upper bound of the fission reactor data, and the uniform elongation becomes close to the lower bound of the database. This extra strengthening is attributable to the higher helium and hydrogen contents generated by spallation reactions. Using nanoindentation technique, room temperature hardness data have been obtained for 316LN stainless steel specimens after irradiation with iron, helium, and hydrogen ions at 200 °C [21]. The data indicated that the additional hardening effect from helium (hydrogen) bubbles became significant at helium concentrations above 1 at.%. In the spallation condition, the helium concentration at the highest dose of 11 dpa was about 0.1 at.% [3–5]. Thus, some strengthening contribution due to the presence of the gases is expected at the highest dose. This extra strengthening from the gases is noticeable in room temperature tests but is expected to extend to more elevated test temperatures. The temperature effects noted herein for the yield strength of EC316LN steel are nearly independent of dose in the range 0–1.87 dpa. This trend might persist to higher doses.

3.2. 9Cr–2WVTa ferritic/martensitic steel

Engineering stress–strain curves for 9Cr–2WVTa ferritic/martensitic steel are displayed in Fig. 5, and the engineering tensile data are listed in Table 3. Irradiation hardening in the ferritic/martensitic steel was strong but less than in the austenitic stainless steel; the yield strengths at 2.53 dpa were less than two times those for unirradiated specimens. All the irradiated specimens displayed plastic instability at yield. This was anticipated from previous tensile data for low doses, which found that at room temperature the critical dose to prompt plastic instability at yield is about 0.1 dpa for the alloy [4]. Consequently, the uniform elongations are near zero and the ultimate tensile strengths equal the yield strengths [22–24].

The effects of test temperature on the tensile properties are weaker in the 9Cr–2WVTa steel than in the EC316LN stainless steel. The ferritic/martensitic steel saw about 10% reduction in the yield strength by increasing test temperature from 20 to 164°C. The increase of test temperature caused about 20% reduction in uniform elongation before irradiation but little difference in ductility after irradiation.

3.3. Strain-hardening behavior in austenitic stainless steels

Figs. 6–8 present true stress (σ)–true strain (ε) curves and strain-hardening rate ($d\sigma/d\varepsilon$) curves for EC316LN stainless steel. In the unirradiated EC316LN stainless steel no yield drop was discerned and the true stress increased steadily with increasing true strain. Very high strain-hardening rates were calculated for the initial small plastic strains because the unirradiated steel showed a continuous yielding, a smooth transition from a high-modulus elastic deformation to plastic deformation without an apparent yield point. The strain-hardening rate decreased with increasing strain but was above the true stress–true strain curve until plastic instability occurred.

It is assumed that the plastic instability or necking initiates at the intersection of the σ vs. ε curve and the $d\sigma/d\varepsilon$ vs. ε curve [25]; i.e., Considere's criterion is applied to obtain the true strain to plastic instability:

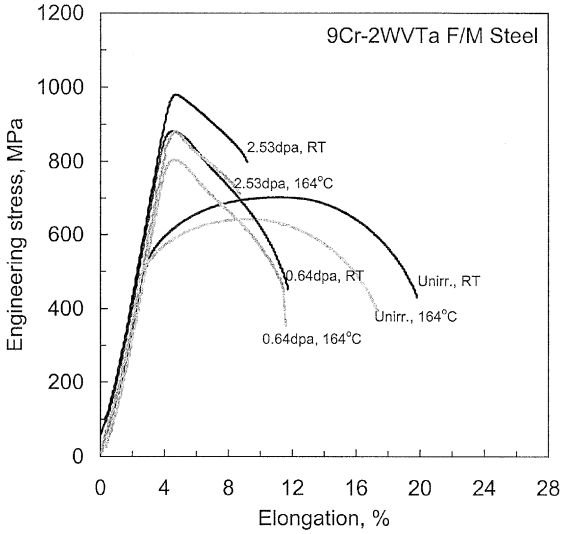

Fig. 5. Engineering stress–strain curves of 9Cr–2WVTa ferritic/martensitic steel after irradiation to labeled doses in spallation environments.

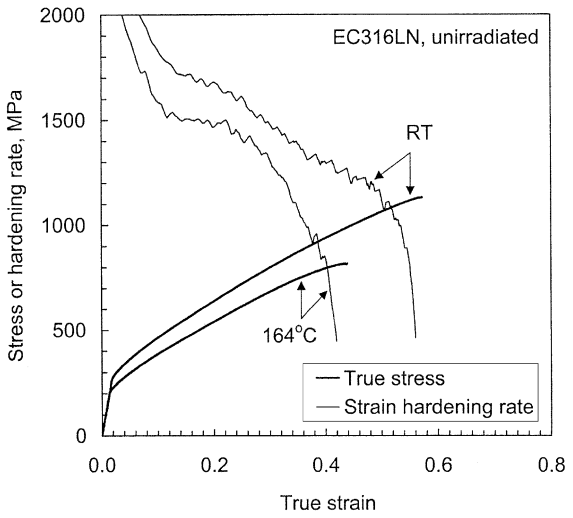

Fig. 6. True stress vs. true strain and strain-hardening rate vs. true strain curves of EC316LN stainless steel before irradiation.

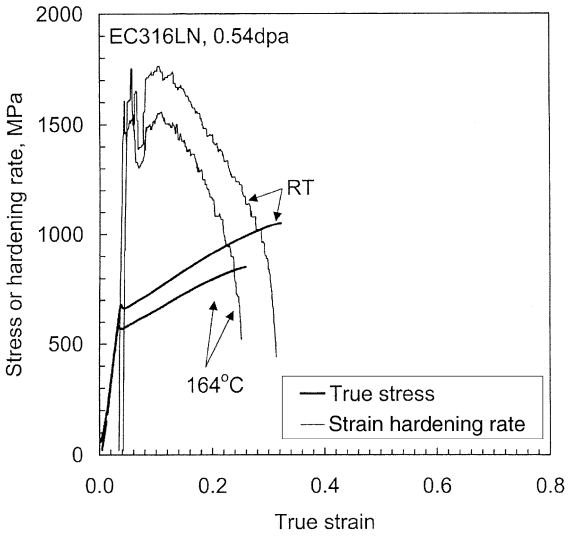

Fig. 7. True stress vs. true strain and strain-hardening rate vs. true strain curves of EC316LN stainless steel after irradiation to 0.54 dpa.

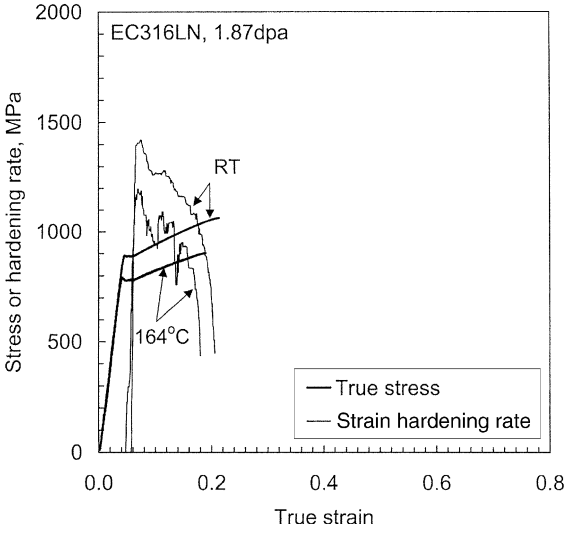

Fig. 8. True stress vs. true strain and strain-hardening rate vs. true strain curves of EC316LN stainless steel after irradiation to 1.87 dpa.

$$\sigma = \frac{d\sigma}{d\varepsilon}. \quad (1)$$

Fig. 6 shows that the true plastic strains at the intersections are about 0.49 and 0.39 for the unirradiated specimens tested at 20 and 164 °C, respectively. Note that the values for true stress and strain-hardening rate become invalid after the onset of plastic instability because of invalidity of true strain values.

As illustrated in Figs. 7 and 8, irradiation changed the shapes of true stress–true strain and strain-hardening rate vs. strain curves at low strains. At both test temperatures the irradiated stainless steel showed small yield drops within a narrow strain range, in which strain-hardening rates were negative. These early low strain portions of the strain-hardening rate vs. strain curves corresponding to elastic deformation and yield drop are omitted in Figs. 7 and 8. After the yield drops, however, the strain-hardening rate recovered quickly to positive value and followed similar curve shapes to those of the unirradiated specimens, although strain-hardening rate was lowered with increasing dose. In Figs. 7 and 8 several intersections exist between true stress–true strain curve and strain-hardening rate curve; at least, one on recovery from negative hardening due to the yield drop and another at the onset of plastic instability. To determine a point at which plastic instability was initiated, the last intersection was assumed to be responsible for the real necking. At doses of 0.54 and 1.87 dpa the true strains to plastic instability were in the range 0.11–0.25.

Large temperature effects were observed on both irradiation-induced strengthening and strain-hardening rate. A 140 °C increase in test temperature lowered the true-stress levels by 10–20% and reduced the strain-hardening rate more significantly, resulting in reductions of uniform strain and instability stress. However, all EC316LN stainless steel specimens irradiated to 0.54 or 1.87 dpa retained positive strain-hardening rate.

At room temperature, the EC316LN stainless steel retained a strong positive strain-hardening capability in the dose range of 0–11 dpa [2–5]. An analysis of the dose dependence of yield stress, instability stress, and fracture stress [5] indicated that the dose to plastic instability at yield would have been about 18 dpa for the EC316LN stainless steel at room temperature. However, the LANL results on 316L stainless steel [6,7], irradiated in the same LANSCE–APT experiment with the present EC316LN stainless steel, showed that the steel experienced a prompt necking at yield at 164 °C after irradiation to 8.7 dpa. At 164 °C, therefore, the dose to a prompt plastic instability at yield must have been equal to or less than 8.7 dpa. In the present work we predicted true strains to plastic instability for both EC316LN and 316L alloys by analyzing existing tensile curves [2–6] and gave the values for uniform true strain at 5 dpa. This is the recommended dose at which the first SNS target modules will be removed from service.

Considere's criterion [25], $\sigma = d\sigma/d\varepsilon$, was applied to determine the true strain to plastic instability, or true strain to necking, rather than reading the uniform elongation at the ultimate tensile strength point. This is because the true strain to plastic instability can be clearly defined on the true stress–true strain and strain-hardening curves by applying Considere's criterion, while the uniform elongation is not easily determined when the

engineering stress–strain curve is nearly flat during uniform deformation. In some irradiated specimens the ultimate tensile strength may be coincident with the yield strength although the material shows positive strain hardening in the true stress unit after a yield drop [3,6]. If the yield drop is large but the strain hardening after the yield drop is very modestly positive, the strength after yield cannot reach the yield strength level until the specimen starts necking. This is because the reduction of cross-sectional area due to uniform deformation offsets positive strain hardening, producing an almost flat engineering stress–strain curve before necking occurs. This type of behavior was observed in the LANL 316 steel tested at 164 °C and shown in Figs. 9 and 10. Applying Considere's criterion, values of 0.018 and 0.033 were determined for true strains to plastic instability at doses of 2.9 and 4.1 dpa, respectively. As explained above, the engineering stress–strain curves in Figs. 9 and 10 are almost flat in the true uniform strain range.

True plastic strain to plastic instability was evaluated for all EC316LN and 316L stainless steel specimens that exhibited uniform deformation. Existing room temperature data for EC316LN steel [5] and new data for EC316LN and 316L steels are regrouped into three data sets with respect to test temperatures: 20, 50, and 164 °C, as listed in Table 4, and used for producing regression curves for the test temperatures. Fig. 11 shows the variation of true strains to plastic instability with dose for each temperature. Trend lines were obtained in the forms of exponential functions, which gave good regression results for the ductility vs. dose data, and were used for interpolations. Comparing the curves indicates that test temperature has a large effect on the dose dependence of true strain to plastic instability in austenitic stainless steels. Reduction in ductility due to irradiation was more significant at 50 and 164 °C than at 20 °C. Interpolations to 5 dpa gave about 0.163, 0.042 and 0.018 for true strains to plastic instability at 20, 50 and 164 °C, respectively. These results predict that the 316 stainless steels will not experience a prompt necking at yield at temperatures of 164 °C or below until the dose reaches higher than 5 dpa, as shown in Fig. 11.

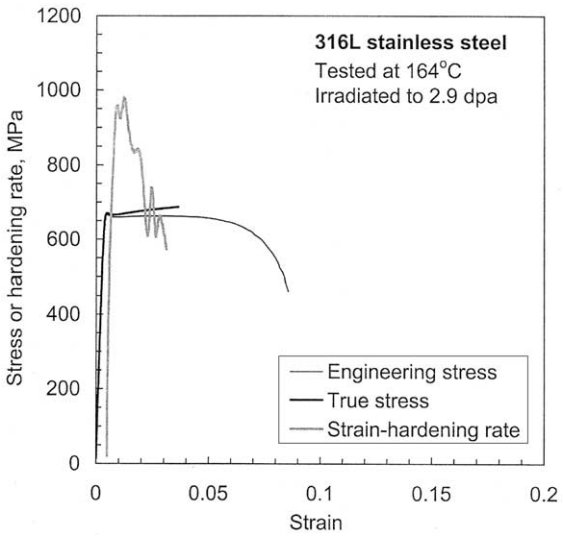

Fig. 9. Comparison of engineering stress–strain, true stress–true strain and strain-hardening rate vs. true strain curves of 316L stainless steel at 164 °C after irradiation to 2.9 dpa.

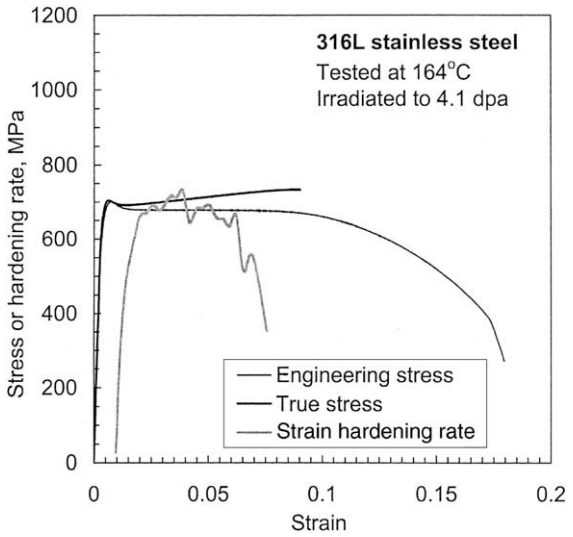

Fig. 10. Comparison of engineering stress–strain, true stress–true strain and strain-hardening rate vs. true strain curves of 316L stainless steel at 164 °C after irradiation to 4.1 dpa.

Table 4 and Fig. 11 also show that for unirradiated stainless steels uniform elongation is strongly affected by test temperature. This is confirmed by ongoing experiments at ORNL on unirradiated 316LN and 304L stainless steels, which display large (40%) reductions in uniform elongation when the test temperature is raised from 0 to 200 °C [26].

3.4. Strain-hardening rate during necking

When the 316L stainless steel was tested at 164 °C after irradiation to above 8 dpa, deformation was localized from the beginning stage of plastic deformation [6,7]. This prompt plastic instability resulted in very small uniform strains of less than 0.5%, consistent with Fig. 11. There has been a question about the strain-hardening behavior after the plastic instability at yield [25,27,28]. Since it is impossible to calculate true strain and true stress data at the neck without its cross-sectional area data, the dimensional change of the neck should be measured to investigate the strain-hardening behavior over the necking process. van Osch and de

Table 4
True strain to plastic instability in 316L and EC316LN stainless steels

ID mark	Material (Origin)	dpa	Test temperature (°C)	True strain to plastic instability
E15	EC316LN (ORNL)	0	20	0.434
316-1	316L (LANL)	0	20	0.438
E12	EC316LN (ORNL)	0	20	0.494
E7	EC316LN (ORNL)	0.45	20	0.292
E51	EC316LN (ORNL)	0.54	20	0.248
E8	EC316LN (ORNL)	0.65	20	0.287
E1	EC316LN (ORNL)	0.86	20	0.296
E4	EC316LN (ORNL)	1.11	20	0.237
E9	EC316LN (ORNL)	1.36	20	0.290
E55	EC316LN (ORNL)	1.87	20	0.129
E2	EC316LN (ORNL)	2.43	20	0.180
E5	EC316LN (ORNL)	2.53	20	0.231
E6	EC316LN (ORNL)	3.64	20	0.211
E3	EC316LN (ORNL)	10.67	20	0.088
316-5	316L (LANL)	0	50	0.383
1A1a	316L (LANL)	0.09	50	0.190
24-6-9	316L (LANL)	1	50	0.232
24-5-1	316L (LANL)	1.2	50	0.179
24-6-8	316L (LANL)	2.9	50	0.199
4-6-5	316L (LANL)	8.8	50	0.007
316-7	316L (LANL)	0	164	0.297
E19	EC316LN (ORNL)	0	164	0.387
E54	EC316LN (ORNL)	0.54	164	0.204
E50	EC316LN (ORNL)	1.87	164	0.116
4-6-9	316L (LANL)	2.9	164	0.018
24-6-6	316L (LANL)	4.1	164	0.033
4-6-7	316L (LANL)	8.7	164	0.003
4-6-6	316L (LANL)	9.2	164	0.002

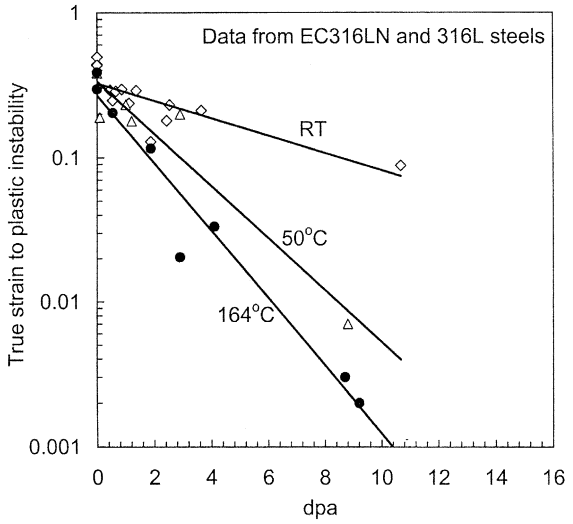

Fig. 11. Dose dependence of true strain to plastic instability.

Vries [27] have measured the RA and calculated true stress and true strain for a V–4Cr–4Ti alloy. In this result, the specimen neutron-irradiated to about 6 dpa and tested at 327 °C displayed prompt necking at yield, however, both the irradiated and unirradiated specimens showed similar positive strain-hardening rates after the onset of necking [27].

RA, as a percentage change from original area to final cross-sectional area after fracture, has been measured for selected specimens, including three 316L stainless steel specimens [19]. Photographs of fracture surfaces were obtained by scanning electron microscopy to measure the final cross-sectional areas. The RA values for 316L stainless steel were in the range 63–73%. Using those RA measurements and tensile test data, we have attempted to calculate the strain-hardening rate during necking. For simplicity, linear hardening is assumed for the true stress–true strain curve of the necking deformation [27,28]:

$$\sigma = \sigma_u + h_n(\varepsilon - \varepsilon_u), \tag{2}$$

where σ_u is the instability stress, h_n is the strain-hardening rate during necking, ε_u is the true strain to plastic instability (true uniform strain).

We can also read fracture strength, S_f, from the engineering stress–strain curve. Then the true fracture strain, ε_f, and true fracture stress, σ_f, can be calculated by

$$\varepsilon_f = \ln\left(\frac{1}{1 - \mathrm{RA}/100}\right), \tag{3}$$

$$\sigma_f = S_f e^{\varepsilon_f}. \tag{4}$$

Using these parameters, h_n is expressed by

$$h_n = \frac{S_f e^{\varepsilon_f} - \sigma_u}{\varepsilon_f - \varepsilon_u}. \tag{5}$$

Strain-hardening rates during plastic instability deformation for three 316L specimens are listed in Table 5, along with results for other parameters. Indeed, our result on strain-hardening behavior agrees with van Osch and de Vries' result on V–4Cr–4Ti alloy [27]; all calculated values for strain-hardening rate are decisively positive. Table 5 also shows that the average strain-hardening rate for necking deformation, h_n, is similar to the strain-hardening rate at onset of necking ($= \sigma_u$). It is interesting to note that the h_n value for the specimen irradiated to 9.2 dpa, which showed prompt necking at yield, can retain a high strain-hardening rate of about 800 MPa during plastic instability.

The result of the high strain-hardening rates for necking deformation is seemingly contrary to the fact that, as indicated in Figs. 6–10, the strain-hardening rate decreases rapidly over the uniform strain range. Assuming that the strain-hardening rate continues to decrease during necking at the same rate, it will become a small positive value or most likely a negative value at fracture strains as high as those in Table 5. However, two complicating factors need to be considered. First, a multi-axial stress state is developed by the geometry of the necked region [27–29]. Since we calculate the true stress values for the neck by dividing applied load by cross-sectional area, the calculated true stress is not the equivalent stress that describes uniaxial uniform deformation but is the axial stress component in the loading direction. It has been shown that this axial stress component can be much higher than the equivalent stress at a given strain [25,28,29], depending on specimen geometry. Second, the complexities of geometry and stress state in the necked region would activate additional dislocation slip systems or even different deformation mechanisms of the material. This can help to sustain a high strain-hardening rate, which usually falls during uniform deformation. Although the current data on strain-hardening rate should be revised in terms of equivalent stress, it is encouraging that the austenitic stainless steels are expected to retain positive hardening during instability deformation after irradiation to at least 9 dpa.

4. Summary and conclusions

Temperature effects on the tensile properties of EC316LN austenitic stainless steel and 9Cr–2WVTa ferritic/martensitic steel were investigated after proton and neutron irradiation to doses up to 2.53 dpa. Tensile testing was performed at two temperatures, 20 and 164 °C. Further, the strain-hardening behavior was analyzed for EC316LN and 316L alloys to study temperature effects and to obtain true strains to plastic instability. The results of the testing and analysis are summarized as follows:

1. All test materials showed significant radiation-induced hardening and loss of ductility due to irradiation. In the engineering stress–strain curves the EC316LN stainless steel maintained notable strain-hardening capability while the 9Cr–2WVTa ferritic/martensitic steel posted negative hardening.
2. In the EC316LN stainless steel, increasing the test temperature from 20 to 164 °C decreased the strength by 13–18% and reduced the ductility by 8–36%. The effect of test temperature in the 9Cr–2WVTa ferritic/martensitic steel was less significant than in the EC316LN stainless steel.
3. At doses less than about 1 dpa the tensile data of the LANSCE-irradiated stainless steels were in line with the fission reactor database for 316 stainless steels irradiated and tested at temperatures below 200 °C. However, extra strengthening induced by helium and hydrogen contents is evident in some specimens irradiated to above about 1 dpa.

Table 5
Strain-hardening rate on plastic instability in irradiated 316L stainless steel

ID mark	dpa	RA (%)	ε_f	ε_u	σ_u (MPa)	S_f (MPa)	h_n (MPa)
24-5-1[a]	1.2	72.9	1.32	0.182	933	580	1090
24-6-6[b]	4.1	82.7	1.75	0.004	705	291	560
4-6-6[b]	9.2	63.6	1.00	0.002	859	613	800

[a] Tested at 50 °C.
[b] Tested at 164 °C.

4. The plastic instability analysis results indicated that modest increase in tensile test temperature has large effects on the dose dependence of true strain to plastic instability in austenitic stainless steels. Interpolations with true uniform strain vs. dpa data showed that the 316 stainless steels would retain more than 1% uniform strain after irradiation to 5 dpa for test temperature up to 164 °C. Much of this temperature dependence stems from an inverse temperature effect on uniform elongation in the unirradiated stainless steels.
5. Calculations on strain-hardening rate during plastic instability predicted that the austenitic stainless steels would retain positive hardening capability during necking after irradiation to at least 9 dpa. This positive hardening capability was explained by the complexities of geometry and stress state in the necked region, which would activate additional dislocation slip systems or even different deformation mechanisms.

Acknowledgements

This research was sponsored by the US Department of Energy, Office of Science, UT-Battelle, LLC, managing Spallation Neutron Source Activities under contract no. DE-AC05-00OR22725. The work at LANL was sponsored by the US Department of Energy under contract no. W-7405-ENG-36 managed by the University of California. We would like to thank Dr W. Sommer of LANL for arranging the collaborative irradiations on which this work is based and Drs R.L. Klueh and D.T. Hoelzer for technical review of the manuscript.

References

[1] L.K. Mansur, T.A. Gabriel, J.R. Haines, D.C. Lousteau, J. Nucl. Mater. 296 (2001) 1.
[2] K. Farrell, T.S. Byun, Spallation Neutron Source Project Report: SNS/TSR-193, Oak Ridge National Laboratory, May 2000.
[3] K. Farrell, T.S. Byun, J. Nucl. Mater. 296 (2001) 129.
[4] K. Farrell, T.S. Byun, Spallation Neutron Source Project Report: SNS/TR-211, Oak Ridge National Laboratory, January 2001.
[5] T.S. Byun, K. Farrell, E.H. Lee, J.D. Hunn, L.K. Mansur, J. Nucl. Mater. 298 (2001) 269.
[6] S.A. Maloy, M.R. James, G. Wilcutt, W.F. Sommer, M. Sokolov, L.L. Snead, M.L. Hamilton, F. Garner, J. Nucl. Mater. 296 (2001) 119.
[7] S.A. Maloy, TPO-RGN-0013, Los Alamos National Laboratory, January 1999.
[8] K. Farrell, SNS/TSR-0036, Oak Ridge National Laboratory, March 1998.
[9] W.F. Sommer, in: Proceedings of the International Workshop on Spallation Materials Technology, Oak Ridge, TN, April 23–25, 1996.
[10] S.A. Maloy, W.F. Sommer, R.D. Brown, J.E. Roberts, J. Eddleman, E. Zimmermann, G. Willcutt, in: Proceedings of the Symposium on Materials for Spallation Neutron Sources, Orlando, FL, Feb. 9–13, 1997, Minerals, Metals and Materials Society, Warrendale, PA, 1998, p. 131.
[11] J.E. Pawel, A.F. Rowcliffe, G.E. Lucas, S.J. Zinkle, J. Nucl. Mater. 239 (1996) 126.
[12] D.W. Kim, W.S. Ryu, J.H. Hong, S.K. Choi, J. Mater. Sci. 33 (1998) 675.
[13] L. Shi, D.O. Northwood, Acta Metall. Mater. 43 (1995) 453.
[14] M.S. Wechsler, M.H. Barnett, D.J. Dudjiak, L.K. Mansur, L.A. Charlton, J.M. Barnes, J.O. Johnson, in: Proceedings of the Symposium on Materials for Spallation Neutron Sources, Orlando, Florida, February 9–13, 1997, Minerals, Metals and Materials Society, Warrendale, PA, 1998, p. 23.
[15] M.H. Barnett, M.S. Wechsler, D.J. Dudziak, L.K. Mansur, B.D. Murphy, J. Nucl. Mater. 296 (2001) 54.
[16] R.E. Prael, H. Lichtenstein, User Guide to LCS: The LAHET Code System, Los Alamos National Laboratory, Los Alamos, NM, 1989.
[17] R.E. Prael, D.G. Madland, LAHET Code System Modifications for LAHET 2.8, Los Alamos National Laboratory, Los Alamos, NM, 1995.
[18] M.R. James, S.A. Maloy, W.F. Sommer, P. Ferguson, M.M. Fowler, K. Corzine, in: Proceedings of the Second International Topical Meeting on Nuclear Applications of Accelerator Technology, Gatlinburg, TN, September 20–23, 1998, American Nuclear Society, La Grange Park, IL, 1998, p. 605.
[19] M.L. Hamilton, APT Project Technical Note: TPO-E20-Z-RTT-X-00002, Los Alamos National Laboratory, January 2000.
[20] J.E. Pawel, A.F. Rowcliffe, G.E. Lucas, S.J. Zinkle, J. Nucl. Mater. 239 (1996) 126.
[21] J.D. Hunn, E.H. Lee, T.S. Byun, L.K. Mansur, J. Nucl. Mater. 282 (2000) 131.
[22] Y. Dai, F. Carsughi, W.F. Sommer, G.S. Bauer, H. Ullmaier, J. Nucl. Mater. 276 (2001) 289.
[23] Y. Dai, S.A. Maloy, G.S. Bauer, W.F. Sommer, J. Nucl. Mater. 276 (2000) 513.
[24] K. Shiba, R.L. Klueh, Y. Miwa, J.P. Robertson, A. Hishinuma, J. Nucl. Mater. 283–287 (2000) 358.
[25] G.E. Dieter, in: Mechanical Metallurgy, 3rd Ed., McGraw-Hill, New York, 1986, p. 283.
[26] K. Farrell, T.S. Byun, N. Hashimoto, Unpublished results on Tensile Properties and Deformation Microstructures of 316LN and 304L Stainless Steels at −150 to 200 °C, 2001.
[27] E.V. van Osch, M.I. de Vries, J. Nucl. Mater. 271&272 (1999) 161.
[28] J. Aronofsky, J. Appl. Mech. 18 (1951) 75.
[29] T.S. Byun, E.H. Lee, J.D. Hunn, K. Farrell, L.K. Mansur, J. Nucl. Mater. 294 (2001) 256.